Quantitative Studies on the Polarization Optical Properties of Living Cells

I. Microphotometric Birefringence Detection System

Y. HIRAMOTO, YUKIHISA HAMAGUCHI, YÔKO SHÔJI, and SHUMEI SHIMODA
Biological Laboratory, Tokyo Institute of Technology, Tokyo 152, Japan

ABSTRACT   A method of polarization optical analysis is described in which phase retardation attributable to birefringence of a minute area in a microscopic object is determined. The optical system consists of a polarizing microscope with "rectified" strain-free lenses, a photoelectric detector to determine the intensity of the light passing through a minute window located at the image plane of the specimen, and a stage that moves the specimen at appropriate velocities for scanning. The error resulting from any flare of light emerging from outside of the area to be measured is minimized by limiting the illuminated area. The specimen can be observed during the measurement of light intensity by illuminating the whole microscope field at a wavelength different from that of the light used for the measurement. The retardation of the specimen is determined by comparing the specimen and background intensities as functions of the azimuth of a Brace-Köhler compensator. Alternatively, retardation is obtained directly from the light intensity at a fixed compensator angle, using the theory of polarization optics. The basal noise level for the present apparatus is ~0.03 nm when measuring birefringence of a 4-μm^2 area in 0.1 s, using a X 40, NA 0.65 objective. The noise decreases in inverse proportion to the square root of the area times the duration of measurement.

Polarization optical analysis gives valuable clues to the ultimate structure of living matter and to an understanding of the mechanism of functional changes taking place in living cells. That is so because birefringence is a manifestation of the structural anisotropy of molecules and/or arrangement of molecules, the dimensions of which lie below the limit of resolution of the light microscope. Though information on submicrostructure obtained by polarization microscopy is not as direct as by electron microscopy, the information is gained directly on active living cells and thus the two approaches complement each other.

In most previous investigations, the retardation of an object was determined by seeking the retardation of a variable compensator that extinguished the brightness of the object when introduced in the optical path of the polarizing microscope. However, it is difficult to determine the precise extinction point by eye, so that measurement by densitometry of photomicrographs (e.g., see references 8 and 13) and photoelectric measurement (e.g., see references 1, 2, and 14) have been used. In the former method, many steps separate the determination of densities in the negative film and the determination of light intensity at the image plane of the microscope.

Because the retardation and axes of birefringence are different in different regions of the cell, they should be determined for small areas having uniform birefringence. As pointed out by Naora (10) in microspectrophotometry, the brightness of an area in a microscope field is affected by the flare of light emerging from the surroundings (Schwarzschild-Villiger [SV] effect; see reference 10). This effect can be minimized by inserting a diaphragm in the optical path so as to limit size of the illuminated area. However, because only a small area is illuminated, it is then impossible to observe the entire microscope field.

In the present paper, we report details of an apparatus for determining weak birefringence of minute areas in microscopic objects by a photoelectric method. The SV-effect is minimized by reducing the illuminated area by inserting a small window in the optical path; the entire microscope field can be observed, without affecting the photoelectric measurement, by illuminating it with light of a different wavelength. In the accompanying

paper (5), we report localized birefringence measurements in dividing sea urchin eggs using this apparatus.

MATERIALS AND METHODS

Birefringence Detection System

The birefringence detection system consists of a Nikon Apophot microscope (Nippon Kogaku K. K., Tokyo, Japan) equipped with rectified strain-free optics (7), a light source to illuminate a limited area for measurement, another light source for observation of the entire microscope field, and a photoelectric detector (Fig. 1). The specimen (S), between a cover slip and a strain-free slide placed on the stage (ST), was illuminated by red light for observation and photography, and by a small spot of green light for photoelectric measurement. The light for observation originated from the built-in light source of the microscope ($S1$, a Xenon lamp, UXL-151D; Ushio Electric Inc., Tokyo, Japan); then passed through a heat-absorbing filter ($F1$), a color filter ($F2$) absorbing rays of short wavelengths (<600 nm), an optical system for Köhler illumination ($L1-L6$), a dichroic mirror ($DM1$), a polarizer (P), a compensator (C), and a rectified condenser (RC); and finally illuminated the entire microscope field. The light for measurement emerged from the second light source ($S2$), a super-high-pressure mercury lamp (USH-102D; Ushio Electric Inc.), then passed through a collector lens ($L7$), a heat-absorbing filter ($F3$), an interference filter ($F4$) for transmitting 546-nm wavelength light, and a minute rectangular window ($W1$); was reflected by the dichroic mirror ($DM1$); then passed along the same path as that of the red light; and illuminated a minute rectangular area in the specimen.

The mica compensator (C) (Brace-Köhler type, 27.7 nm [0.319 radian] or 24.7 nm [0.284 radian] for 546-nm monochromatic light; Nippon Kogaku K. K.) was rotated with a micromotor attached to a potentiometer, which converted the compensator angle to voltage. The condenser (RC) was fitted with rectified optics (cf. reference 7) ($f = 8$ mm, 1.15 NA or $f = 16$ mm, 0.52 NA; Nippon Kogaku K. K.). The window ($W1$), which was custom made by Narishige Scientific Instrument Laboratory, Tokyo, Japan, consisted of a pair of slits set at right angles to each other. The width of each slit could be varied from 30 to 750 μm. $W1$ was positioned so that its image was focused by the condenser (RC) at the plane of the specimen (S). Because the size of the image was reduced to 1/30 of the size of the window when the condenser of 8-mm focal length was used, the width of the illuminated area could be varied from 1 to 25 μm. When the rectified, long (8-mm) working distance condenser of 16-mm focal length was used, the illuminated area could be varied from 2 to 50 μm in width. The position of $W1$ was centered on the optical axis with a screw device, during observation through the inclined tube (IT), or through the viewfinder (VF) of the microscope camera (MC).

The image of the specimen was formed on the image plane in the viewfinder (VF) or on the film in the microscope camera (MC) through a Nikon rectified objective (OB; × 10/0.30, × 20/0.40, × 40/0.65 or × 100/1.25), an ocular (OC; HKW [high eye-point compensating wide-field ocular] × 10; Nippon Kogaku K. K.), a dichroic mirror ($DM2$), and the lens ($L10$ or $L11$) of the microscope camera. The dichroic mirrors ($DM1$, $DM2$), which were supplied by Nippon Kogaku K. K., passed long-wavelength light and reflected short-wavelength light (50% transmission at 570-nm light). Because practically all of the red light for observation and a small fraction of the green light for measurement passed through the dichroic mirror ($DM2$), the area illuminated by the green light could be recognized at the center of the red-illuminated microscope field when observed through the viewfinder (VF). Most of the green light was reflected by the dichroic mirror ($DM2$) and formed the image of $W1$ on the plane of the second window
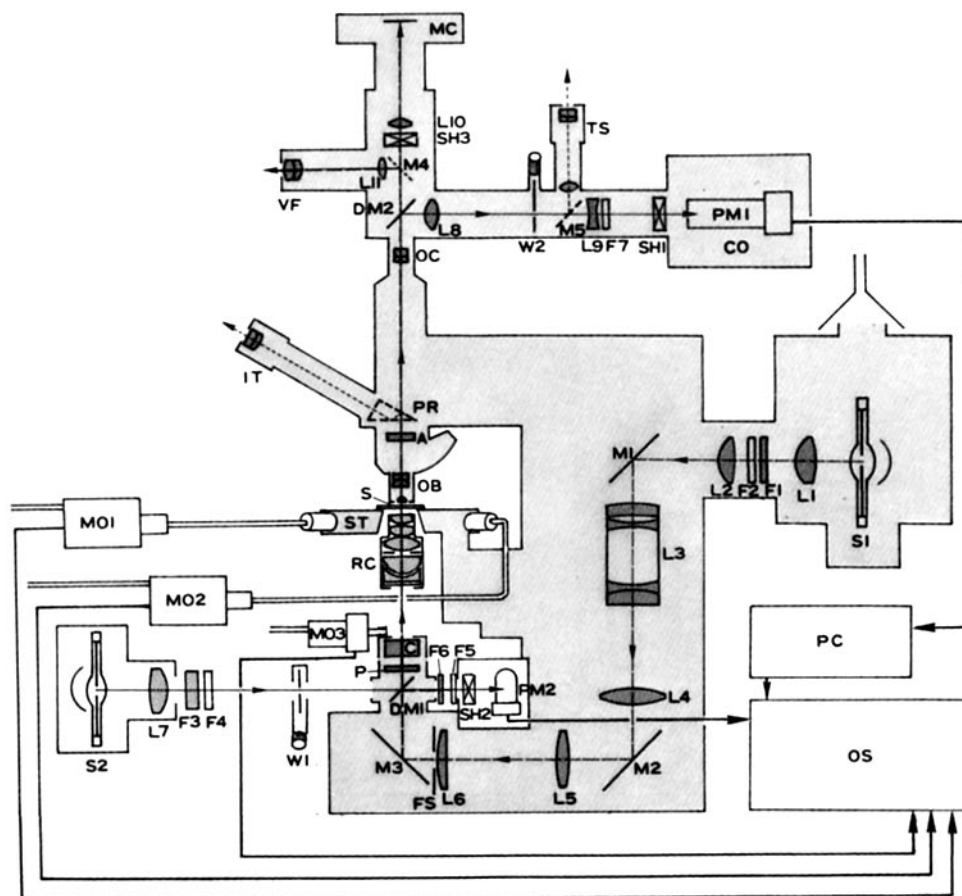

FIGURE 1 Diagram of the optical and recording systems. A, analyzer; C, compensator; CO, photomultiplier cooler; DM1, DM2, dichroic mirrors; F1, F3, heat-absorbing filters; F2, red filter for absorbing rays of short wavelengths (<600 nm); F4, F5, F7, interference filters for passing 546-nm wavelength rays; F6, neutral density filter; FS, field stop; IT, inclined tube for observation; L1–L11, lenses; M1–M5, mirrors; MC, microscope camera; MO1, MO2, MO3, micro-motors with potentiometers; OB, objective; OC, ocular; OS, oscilloscope; P, polarizer; PC, photoncounter; PM1, PM2, photomultipliers; PR, prism; RC, rectified condenser; S, specimen; S1, light source for observation (xenon arc lamp); S2, light source for measurement (high-pressure mercury arc lamp); SH1–SH3, shutters; ST, microscope stage; TS, telescope for adjusting the position of W2; VF, viewfinder of the microscope camera; W1, W2, windows for limiting the light beam for measurement.

(*W2*) after passing through a lens (*L8*; f = 12.5 cm). *W2* consisted of a pair of slits set at right angles to each other, and the width of each slit could be varied from 0 to 5 mm, which corresponded to 0–25 μm at the specimen plane when a × 40 objective and a × 10 ocular were used. Before experimentation, the position of *W2* was adjusted with a screw device and position to the axis of the optical system by observation through a telescope (*TS*) that was removed from the optical path during measurement. The size of *W1* was adjusted so that its image at the plane of *W2* was slightly larger than the area of *W2*, as will be described later. The light passing *W2* was cast on the photocathode of a photomultiplier (*PM1*) after a slight divergence by a lens (*L9*). An interference filter (*F7*) could be introduced to cut out the red light that strayed into the optical path, although it was usually not necessary because the intensity of the stray light was very small, as is mentioned later.

The intensity of light was determined by counting the number of photoelectrons emitted at the photocathode of the photomultiplier (*PM1*; R464, Hamamatsu TV Co., Hamamatsu, Japan) for each given duration, which varied from 5 ms to 200 s, with a photon counter (*PC*; PC-545A with preamplifier IA551, NF Circuit Design Block Co., Yokohama, Japan) and was displayed with an oscilloscope (*OS*; 5103N, Sony-Tektronix Co., Tokyo, Japan). The photomultiplier (*PM1*), which was mounted in a photomultiplier cooler (*CO*; C659, Hamamatsu TV Co.) equipped with a shutter (*SH1*), was kept at −20°C during measurement to minimize dark current. The relation between the number of photoelectrons emitted at the photocathode and the compensator angle was displayed on the oscilloscope (*OS*), by displaying the output analog signal of the photon counter in the vertical axis and the voltage proportional to the compensator angle in the horizontal axis. The fluctuation of the intensity of the light used for measurement was monitored by receiving the light that passed through the dichroic mirror (*DM1*), neutral density filter (*F6*), and 546-nm interference filter (*F5*; for transmitting 546-nm wavelength light), with a photomultiplier (*PM2*; 1P21, Tokyo Shibaura Electric Co., Tokyo, Japan) and recording it with the oscilloscope (*OS*) (cf. record *L* in Fig. 4*b*). The intensity of light recorded by the main photomultiplier/photon counter/oscilloscope system was corrected after consideration of this fluctuation of the intensity of the light source, when necessary. The intensity of light received by the monitoring photomultiplier (*PM2*) was scarcely affected by the observation beam. This indicates that the light from S1 was almost completely cut out by the filters and dichroic mirrors before entering the photomultiplier (*PM2*), so that the light recorded by the PM2-oscilloscope system quite accurately indicates the relative intensity of the measuring beam.

The microscope stage (a Nikon rotating stage type H, modified by Narishige Scientific Instrument Laboratory) could be moved with micrometer screws in 45° and 135° directions with respect to the vibration direction of the polarizer to drive the specimen on the stage in these directions to traverse the light beam. The screws were driven with micromotors each attached to a potentiometer transducing the rotation angle of the screw to voltage. In some cases, the movements of the micrometer screws in the control units (*MO1*, *MO2*) were transmitted to the stage by oil pressure through tubings connecting the stage and the control units. In those cases, the rotating angles of the micrometer screws were converted to voltage with potentiometers. The speed of the stage could be varied from 0.25 to 10 μm/s.

Retardation Measurement

The specimen was set on the stage so that its azimuth lay at 45° with respect to the vibration direction of the polarizer. The portion to be measured was placed at the center of the microscope field, which was illuminated by the beam of green light. The analyzer (*A* in Fig. 1) was set so that its vibration plane was perpendicular to that of the polarizer (*P*). The intensity of light measured by the photomultiplier/photon counter/oscilloscope system (*PM1/PC/OS*) changed with the compensator angle as shown by *S* in Fig. 2. In this case, the specimen was a bundle of fibrils of glycerinated muscle of the crab *Sesarma haematocheir*, and the area to be measured was 0.5 × 2 μm on the I band of the bundle. When the specimen was removed from the center of the microscope field, so that the measuring beam passed through the background outside the specimen, the intensity-compensator angle relation changed as shown by *B* in Fig. 2.

According to the theory of polarization optics (cf. reference 9), when a doubly refracting plate is placed between the crossed polarizer and analyzer, the intensity (I_1) of light emerging from the analyzer is given by

$$I_1 = I_0 \sin^2 2\gamma_1 \sin^2 \frac{\delta_1}{2}, \tag{1}$$

where γ_1 and δ_1 are the azimuth and the phase difference of the plate, respectively, and I_0 is the intensity of the light emerging from the polarizer. When another doubly refracting plate without absorbance is inserted between the crossed polarizer and analyzer, the intensity (I_2) of light emerging from the analyzer is given by
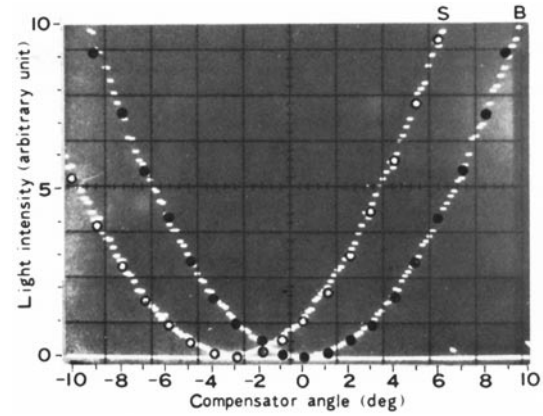

FIGURE 2 Relations between the light intensity and the compensator angle. Trains of white spots are oscillograph records obtained for a 2 × 0.5 μm region in the I band of a small bundle of fibrils isolated from glycerinated muscle of the crab *Sesarma haematocheir* (S) and for an equivalent area in the background (B). Closed and open circles are values calculated from Eqs. 1 and 3.

$$I_2 = I_0 \left[\sin^2 2\gamma_1 \sin^2 \frac{\delta_1}{2} + \sin^2 2\gamma_2 \sin^2 \frac{\delta_2}{2} \right.$$
$$\left. + 2 \sin 2\gamma_1 \sin 2\gamma_2 \sin \frac{\delta_1}{2} \sin \frac{\delta_2}{2} \left\{ \cos \frac{\delta_1}{2} \cos \frac{\delta_2}{2} - \cos 2(\gamma_2 - \gamma_1) \sin \frac{\delta_1}{2} \sin \frac{\delta_2}{2} \right\} \right], \tag{2}$$

where γ_2 and δ_2 are the azimuth and the phase difference of the second plate. When $\gamma_2 = \pi/4$ rad,

$$I_2 = I_0 \left[\sin^2 \frac{\delta_1}{2} \cos \delta_2 \sin^2 2\gamma_1 + \frac{1}{2} (\sin \delta_1 \sin \delta_2 \sin 2\gamma_1) + \sin^2 \frac{\delta_2}{2} \right]. \tag{3}$$

The closed circles on the record *B* in Fig. 2 were obtained by substituting 0.319 rad (retardation of the compensator in this case) for δ_1, the compensator angle for γ_1, and an appropriate value for I_0 in Eq. 1. The open circles on *S* in Fig. 2 were obtained by substituting the same values for δ_1, γ_1, and I_0 and 0.036 rad (2.1°) for δ_2 in Eq. 3. The excellent agreement between the experimental and expected results indicates that the present experimental setup is suitable for microphotometric measurement of birefringence and that the specimen used in the experiment shown in Fig. 2 had a retardation (phase difference) of 0.036 rad (3.1 nm) and displayed little absorbance or light scattering. The slight difference between the experimental results and the expected ones, which is barely noticed near the minima of the curves, may be attributable to stray light introduced by the birefringence of the slide and/or cover slip. If this stray light component is added to the theoretical points, the coincidence of the theory and experiment becomes even better. The light from the specimen often contained stray light (probably caused by rotation of the plane of polarized light at the interface of different refractive indices) and by scattering and birefringence of randomly oriented particles (e.g., protoplasmic vacuoles) in the optical path. In those cases, the light intensity–compensator angle curve was displaced in parallel to the intensity axis as shown in Fig. 3 (*S → S'*). Furthermore, the form of the curve often changed to a less steep one (*S''* in Fig. 2), probably owing to attenuation of light intensity by absorption in the specimen. However, the light intensity–compensator angle curve was well explained by Eq. 3 if the displacement of the curve by stray light and attenuation of light intensity by absorption were taken into account.

If the compensator angle at which the light intensity from the sample becomes minimal (extinction angle) is γ_0, then from Eq. 3

$$\tan \delta_2 = -2 \tan \frac{\delta_1}{2} \sin 2\gamma_0. \tag{4}$$

When both δ_1 and δ_2 are sufficiently small to enable tan δ_2 and tan $\delta_1/2$ to be regarded as δ_2 and $\delta_1/2$, respectively, then

$$\delta_2 = -\delta_1 \sin 2\gamma_0. \tag{5}$$

Therefore, the retardation of the specimen is obtained from the retardation of the compensator (δ_1) and the extinction angle (γ_0) by use of Eq. 4 or 5. This method can be used even when the stray light and the attenuation of light by absorption are present, because γ_0 is not affected by them (cf. Fig. 3).

When the intensity of stray light and light attenuation by absorption in the

specimen are small, the retardation of the specimen can be determined from the light intensity with compensator angle fixed to a definite value, because the intensity is given by Eq. 3 when I_0, δ_1, δ_2, and γ_2 are given. The vertical scale seen at +6° in Fig. 4a indicates retardation values (δ_2) corresponding to various light intensities, which were calculated using δ_1 (0.319 rad), γ_1 (6° = 0.0105 rad), and a value for I, satisfying the reference curve obtained for the background.

This method cannot be used when the intensity of stray light varies between the background and the sample or when the attenuation of the light intensity is not negligible. However, this method can be used if an appropriate isotropic region, where both the intensity of the stray light and the attenuation of the light intensity are practically the same as those of the sample, is found for obtaining the reference curve. In experiments on living cells, the isotropic portion in the sample, rather than the background outside the sample, was often used as the reference for determining the birefringence of the anisotropic portions in the sample.

Because the microscope stage could be moved in directions at 45° and 135° to the vibration direction of the polarizer in the present experimental setup, the distribution of retardation along the 45° and 135° lines could be displayed by
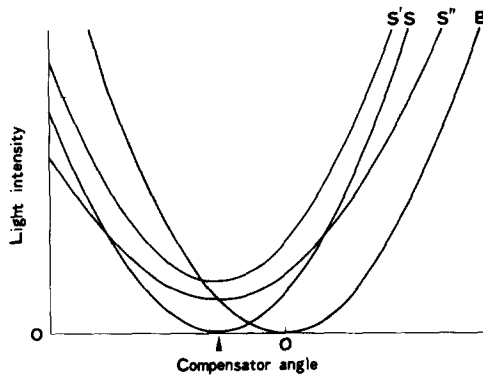

FIGURE 3 Principle of retardation measurement from the extinction angle. The figure shows the relations between light intensity and compensator angle for the background (B) and the sample (S, S', and S''). The relations closely agree with theory of optics as shown by B and S (and B and S in Fig. 2) when the stray light and attenuation of light intensity by absorption, scattering, etc., are negligible. The curve is displaced upwards when stray light is present (S') and changes in its form when attenuation is present (S''). The extinction angle (γ_0) is the same in these cases. The retardation is calculated by Eq. 4.

oscillographic records in which the output of the photon counter was displayed on the vertical axis and voltage representing the rotation angle of the micrometer for moving the stage was displayed on the horizontal axis. Fig. 4b indicates the distribution of retardation along the axis of a mitotic apparatus isolated from an egg of the sand dollar Clypeaster japonicus during the first division.

The Size of the Illuminated Area for Measurement

In the present apparatus, a small rectangular area in the specimen was illuminated by green light (546-nm wavelength) by projecting the image of a small window ($W1$ in Fig. 1) in the light path. The size of the area to be illuminated was determined from the results of the following experiments so that the region for measurement of birefringent retardation was uniformly illuminated and the effect of light emerging from the surroundings (SV effect; see reference 10) was sufficiently small.

In the first experiment, a stage micrometer was placed on the stage, and a region outside the scale of the micrometer was brought to the microscope field after focusing the scale. This region gave an almost uniform brightness over the microscope field, owing to the strain birefringence of the slide. Images of $W1$ were formed at the plane of the specimen after a reduction to 1/30 with the rectified condenser (8-mm focal length) and at the plane of $W2$ after a magnification of 200 with a ×40 rectified objective, ×10 ocular and a relay lens ($L8$). Both $W1$ and $W2$ were square in shape. The sides of the image of $W1$ formed at the $W2$ plane were adjusted to be parallel to the sides of $W2$, and the two images were centered to each other. The measurements gave the distribution of light intensity at the plane of $W2$. Fig. 5 shows a typical example of a series of experiments. In this case, $W1$ was 0.18 mm square (A), 0.15 mm square (B), and 0.12 mm square (C), corresponding to 6 μm square, 5 μm square, and 4 μm square, respectively, at the plane of the specimen and 1.2 mm square, 1 mm square, and 0.8 mm square, respectively, at the plane of $W2$. $W2$ was 0.4 mm square corresponding to 2 μm square at the specimen plane. It can be seen in this figure that: the light intensity is almost uniform in the central region of the image of $W1$ as expected from geometrical optics; light intensity is less at the periphery of the image of $W1$ (0.2–0.3 mm from the edge at the $W2$ plane or 1–1.5 μm at the specimen plane); and appreciable brightness is detected outside the image. We believe that the reduction of the light intensity at the peripheral region and the spread of the light onto the surroundings result from diffraction and the flare of light in the optical system.

In the second experiment, the variation of the light intensity passing through $W2$ was determined when the size of $W1$ was changed. The size of $W2$ was fixed to 0.2 mm square or 0.4 mm square, corresponding to 1 μm square or 2 μm square respectively at the specimen plane, and the image of $W1$ was centered to $W2$. As the size of $W1$ increased, the light intensity sharply increased until the size of the image of $W1$ at the specimen plane became greater by 3 μm than the size of the image of $W2$. As the size of $W1$ was increased further, the light intensity increased
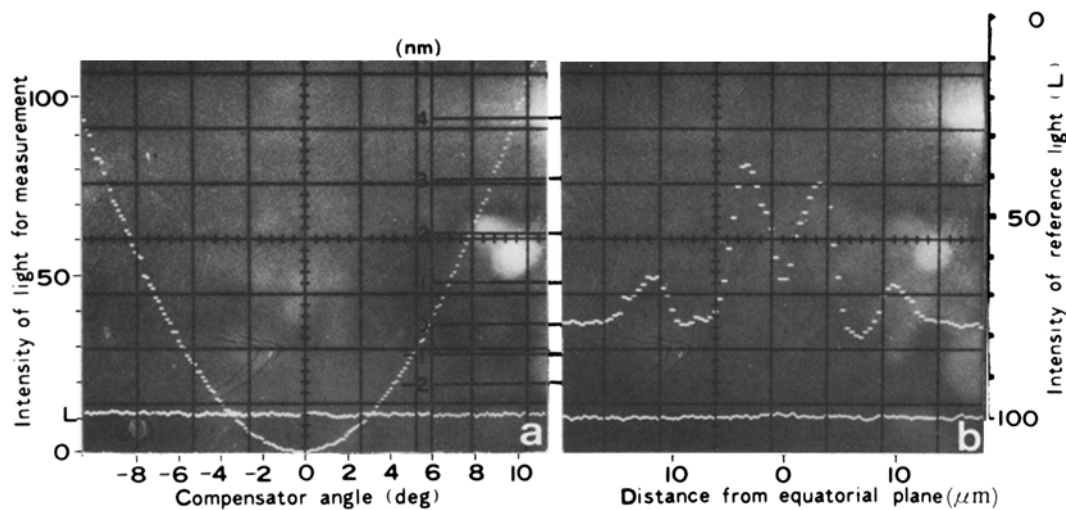

FIGURE 4 Determination of birefringence retardation along the light intensity with fixed compensator orientation. (a). The train of white dots in the oscillographic record indicates the relation between the light intensity of the background and the compensator angle. The brightness of the specimen with given retardation values are calculated for a 6° compensator angle according to Eq. 4, using the data obtained from the relation between the light intensity of the background and the compensator angle (assuming that both the stray light and the attenuation of the light intensity are negligible in the sample). (b) Retardation vs. distance along the spindle axis in a mitotic apparatus isolated from an egg of the sand dollar, Clypeaster japonicus. Record L indicates fluctuation of the light intensity of the light source (cf. scale on the right).

gradually. It is thought that the initial sharp increase in light intensity is attributable to the increase in the incident light on the area to be measured and the gradual increase at greater sizes of W1 is attributable to the increase in flare of light emerging from surroundings of the area to be measured (SV effect). From the above experiments, we decided to use a size of W1 such that the image of W1 at the specimen plane, when centered on the region for measurement, was ~1.5 μm wider all around.

RESULTS AND DISCUSSION

Effects of Numerical Apertures of the Objective and the Condenser on Retardation Measurement

Because objective and condenser lenses with high numerical apertures were used to obtain good resolution in the present apparatus, a question arises whether the retardation value determined with such lenses using oblique rays is different from that determined using paraxial rays. To answer this question, we made retardation measurements with × 40 rectified objective and an 8-mm rectified condenser at various numerical apertures. The numerical aperture of the objective (0.65 without stop) was changed to 0.31 or 0.17 by putting a stop near the "rectifier" attached to the objective. The condenser aperture was set to 0.17, 0.31, or 0.65 using the iris diaphragm attached to the condensor.

An ~5-μm-thick bundle of myofibrils, which was dissected out of glycerinated leg flexor muscle of the crab *Sesarma haematocheir* was placed on a strain-free glass slide and covered with a cover slip. A 4-μm-square region in the I band of the myofibril was illuminated, and the retardation of a 1-μm-square region at its center was determined from the extinction angle displayed by the oscilloscope, using Eq. 5. It was found that the retardation values were almost the same in all the combinations of numerical apertures of the objective and the condenser mentioned above, indicating that retardation measurements were scarcely affected by the difference in the numerical aperture in the present experimental setup.

Sato et al. (12) arrived at the same conclusion using visual compensation determination with rectified objectives of different numerical apertures (× 40/0.65, × 20/0.40, and × 10/0.25).

Limitations of the Present Setup and Applications to Cell Biology

Using the present experimental setup, it is possible to determine small birefringence retardation of microscopic objects as small as 1 μm. The location to be measured can be confirmed by observation through the viewfinder during measurement. The increase in light intensity by illumination of the entire microscope field with red light was <3%, as determined by the photomultiplier/photon counter/oscilloscope system (*PM1/ PC/OS*). The percentage increase was almost constant irrespective of the compensator angle, so that measurements were usually carried out while the entire microscope field was illuminated without using the interference filter (*F7*). The background light intensity attributable to red light could be reduced to <0.1% by inserting the filter (*F2*).

The sensitivity of birefringence determination with the present setup is determined by the number of photoelectrons emitted from the photocathode of the photomultiplier, which depends on the intensity of the light source, the area to be measured on the specimen plane, and the duration of illumination for photon counting. In a typical case where the area to be measured was 4 μm², the duration for photon counting was
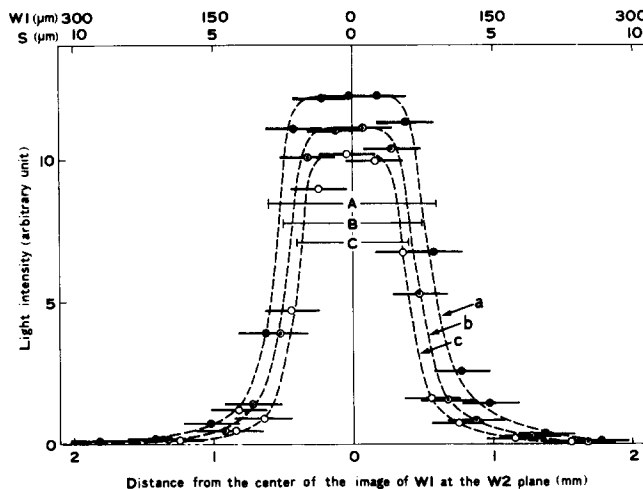

FIGURE 5   Distribution of light intensity at the plane of the second window (*W2* in Fig. 1). Curves *a*, *b*, and *c* are the distributions of light intensity with the first window (*W1*) of three different sizes (0.18-mm square, 0.15-mm square, and 0.12-mm square shown by *A*, *B*, and *C*, respectively). The corresponding sizes of *W1* and the sizes of the image of *W1* at the plane of the specimen are shown by scales *W1* and *S* at the top of this figure.

0.1 s, and the compensator angle was fixed at 6°, the number (*n*) of photoelectrons emitted from the photocathode was ~10^4. Thermal noise generated at the photocathode was minimized by chilling the photomultiplier to −20°C, as mentioned above. Thermal noise resulting from low-energy pulses generated at the dynodes and nonthermal noise resulting from high-energy pulses generated by cosmic rays, etc., were eliminated by circuits in the photon counter. As a result, the noise observed when the light sources were extinguished was 1–2 photoelectrons/s, i.e., 1–2 × 10^{-5} of the signal. Because this noise level is very low, noise in the electrophotometric system results mainly from the fluctuation of emission of photoelectrons from the photocathode. Because a Poisson distribution is observed for the number of photoelectrons emitted, the standard deviation is given by the square root of the number of electrons (which is 100, or 1% of 10^4 in the above example). From the relationship of retardation to light intensity at a fixed compensator angle, 1% deviation of the light intensity corresponds to 0.03-nm retardation. This indicates the approximate limitation for the retardation measurement. A similar figure is obtained when the retardation is determined from the extinction angle of the compensator, because the extinction angle is determined from the mean of two different angles giving the same light intensity.

Because the number of photoelectrons counted is proportional to the area being measured and to the duration of counting, and because the standard deviation is given by the square root of the number, the error is inversely proportional to the square root of the number of photoelectrons emitted. Therefore, the minimum detectable retardation from a sample area of 1 μm² is twice that of a sample area of 4 μm². It increases by $\sqrt{20}$ (≅4.5) times when the duration of photon counting is reduced to 5 ms (the shortest duration in the present setup) instead of 0.1 s. Also, the precision of photoncounting decreases with shorter duration.

Errors resulting from fluctuations in light intensity of the light source (*S2* in Fig. 1) can be corrected by checking the light intensity with a photomultiplier (*PM2* in Fig. 1) as

mentioned above, though the correction usually unnecessary because the fluctuations were very small.

The birefringence (BR) detection apparatus reported here exhibits high resolving power and sensitivity, as demonstrated in Fig. 6, in which Z, H, and M lines as well as A and I bands can be clearly recognized. Because of these qualities and its rapid response, the present setup appears to be exceptionally useful for quantitatively analyzing rapidly changing birefringent structures in living, moving cells.

Comparison of the Present System with Previous Systems for Measuring BR of Microscopic Objects

Three kinds of photometric methods (visual, photographic, and electronic) are used for BR measurement of microscopic objects. The dark-adapted eye is an efficient detector and 10^{-1}–10^{-2} nm of retardation can be detected in a high-extinction polarizing microscope (e.g., see references 6, 7, and 11). Photographic detection methods (e.g., 8 and 13) have a sensitivity comparable to the visual method, but scrupulous care and troublesome procedures are required to obtain reliable results. Neither method is applicable to an object showing rapid motility or fluctuations in BR.

As discussed by Allen et al. (1, 2), the electronic method has various merits in BR measurement as compared with visual and photographic methods, especially in its rapid responsiveness to BR change. The sensitivity of the present system (0.03 nm) is as high as visual and photographic methods when the area is 4 μm^2 and the duration of measurement is 0.1 s, and it increases in proportion to the square root of the area times the duration. The basal noise level in the system (0.002 A for a spot 36 μm in diameter) of Allen et al. (1, 2) and that in the system (0.1 nm for a spot of 30 μm in diameter) of Taylor and Zeh (15) are comparable to that in the present system, if the time constant of each system is taken into consideration. Using the present system, it is possible to detect weak BR retardation of 10^{-3}–10^{-4} nm under best conditions. Also, it is possible to measure BR of an area as small as 1 μm with a time constant as short as 5 ms with an appropriate sensitivity.

One of the distinctive features of the present system is that the image of the specimen and location of the measured spot
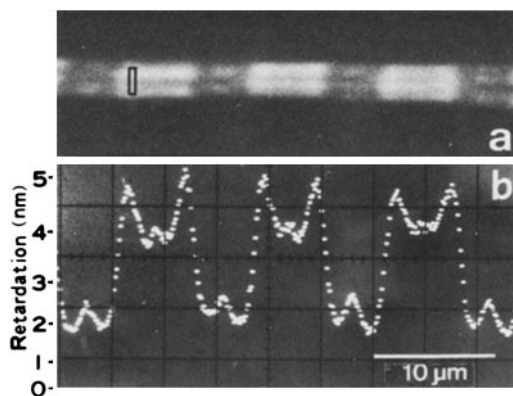

FIGURE 6 Distribution of birefringence retardation along the axis of a bundle of myofibrils dissected from a glycerinated leg muscle of the crab Sesarma haematocheir. Oscillograph record (b) showing the distribution of birefringence along the axis of the bundle shown by the photomicrograph in a. The dimension of the area used in scanning is shown by a small rectangle on the A band of the bundle. Z line, I band, A band, H zone and M line are shown in the record and the photomicrograph. a, × 1,600.

can be continuously monitored during the measurement under consideration of the SV effect, which was neglected in previous investigation. Though the retardation is determined directly from the light intensity or the compensator angle showing minimum light intensity, it may be possible to determine automatically from the phase difference if an electro-optical light modulator is used, as Allen et al. (1, 2) and Taylor (14) described.

The change in BR retardation during contraction has been determined in muscle fibers in detail by use of electronic methods (e.g., see references 3, 4, and 14) suitable for measuring BR retardation considerably larger than the retardation measured by the present system. Although these methods determined BR change of a large area covering many sarcomeres, it is desirable to determine the BR change for individual parts constituting the sarcomere, such as A band, I band and H zone, so that the structural changes during muscular contraction may be understood in more detail. The present system may be useful for this purpose because of its high space and time resolutions.

REFERENCES

1. Allen, R. D., J. Brault, and R. D. Moore. 1963. A new method of polarization microscopic analysis. I. Scanning with a birefringence detection system. J. Cell Biol. 18:223–235.
2. Allen, R. D., J. Brault, and R. Zeh. 1966. Image contrast and phase modulation light methods in polarization and interference microscopy. In Advances in Optical and Electron Microscopy. R. Barer and V. E. Cosslett, editors. Academic Press, Inc., New York. 77–114.
3. Baylor, S. M., and H. Oetliker. 1977. A large birefringence signal preceding contraction in single twitch fibres of the frog. J. Physiol. (Lond.). 264:141–162.
4. Eberstein, A., and A. Rosenfalck. 1963. Birefringence of isolated muscle fibres in twitch and tetanus. Acta Physiol. Scand. 57:144–166.
5. Hiramoto, Y., Y. Hamaguchi, Y. Shôji, T. E. Schroeder, S. Shimoda, and S. Nakamura. Quantitative studies on the polarization optical properties of living cells. II. The role of microtubules in birefringence of the spindle of the sea urchin egg. J. Cell Biol. 89:121–130.
6. Inoué, S. 1961. Polarizing microscope. Design for maximum sensitivity. In The Encyclopedia of Microscopy. G. L. Clark, editor. Reinhold Publishing Co., New York. 480–485.
7. Inoué, S., and W. L. Hyde. 1957. Studies on depolarization of light at microscope lens surface. II. The simultaneous realization of high resolution and high sensitivity with the polarizing microscope. J. Biophys. Biochem. Cytol. 3:831–838.
8. Inoué, S., and H. Sato. 1966. Deoxyribonucleic acid arrangement in living sperm. In Molecular Architecture in Cell Physiology. T. Hayashi and A. G. Szent-Gyorgyi, editors. Prentice-Hall Inc., Englewood Cliffs, New Jersey. 209–248.
9. Jerrard, H. G. 1948. Optical compensators for measurement of elliptical polarization. J. Opt. Soc. Am. 38:35–59.
10. Naora, H. 1955. Microspectrophotometry of cell nucleus stained by Feulgen reaction. I. Microspectrophotometric apparatus without Schwarzschild-Villiger effect. Exp. Cell Res. 8:259–278.
11. Salmon, E. D., and G. W. Ellis. 1975. Compensator transducer increases ease, accuracy, and rapidity of measuring changes in specimen birefringence with polarization microscopy. J. Microsc. (Oxf.). 106:63–69.
12. Sato, H., G. W. Ellis, and S. Inoué. 1975. Microtubular origin of mitotic spindle form birefringence. Demonstration of the applicability of Wiener's equation. J. Cell Biol. 67:501–517.
13. Swann, M. M., and J. M. Mitchison. 1950. Refinements in polarized light microscopy. J. Exp. Biol. 27:226–237.
14. Taylor, D. L. 1979. Quantitative studies on the polarization optical properties of striated muscle. I. Birefringence changes of rabbit psoas muscle in the transition from rigor to relaxed state. J. Cell Biol. 68:497–511.
15. Taylor, D. L., and R. M. Zeh. 1976. Methods for the measurement of polarization optical properties. I. Birefringence. J. Microsc. (Oxf.). 108:251–259.